# Supporting Information

## Maher et al. 10.1073/pnas.0808946106

### SI Methods

**Preparation of Slices.** Mice were deeply anesthetized with isoflurane and then decapitated. Bulbs were rapidly removed and immersed in ice-cold oxygenated (95% $O_2$ and 5% $CO_2$) dissection buffer (in mM): 83 NaCl/2.5 KCl/1 $NaH_2PO_4$/26.2 $NaHCO_3$/22 glucose/72 sucrose/0.5 $CaCl_2$/3.3 $MgSO_4$. Horizontal slices (290 $\mu$M) were cut by using a vibrating blade Vibrotome (VT1000S; Leica), incubated in dissection buffer for 30–45 min at 37 °C, and then stored at room temperature. Slices were visualized using IR differential interference contrast microscopy (DIC) (Zeiss Axioskop) and a CCD camera (XC-ST30; Sony). Individual mitral cells expressing YFP were visualized with epifluorescent illumination and a 40× Zeiss water-immersion (0.75 numerical aperture) objective. We used exclusively mitral cell pairs that projected to the same glomerulus, as confirmed by identification of apical dendrites at the time of recording with Alexa Fluor 594, or with posthoc analysis of biocytin fills by confocal microscopy.

**Naris Occlusion.** Mice [postnatal day (P)1] were deeply anesthetized by inhalation of 2.5% isoflurane in $O_2$. Occlusion was achieved by electrical cautery (Aaron Medical) of the right naris under a dissecting scope. Subsequent scar tissue formation rendered the occlusion permanent, but does not damage the olfactory epithelium directly. Thus, the result the olfactory bulb does not receive natural sensory input, but olfactory receptor neurons or the olfactory nerve axons can still contact the olfactory bulb. Lidocaine gel was applied to reduce any postprocedural pain, and the animal was placed back in its home cage. Naris occlusion was deemed successful when the bulb ipsilateral to the occlusion was smaller than the contralateral bulb (1).

**Electrophysiology.** For all experiments, artificial cerebrospinal fluid (ACSF) was oxygenated (95% $O_2$ and 5% $CO_2$) and contained (in mM): 125 NaCl/25 $NaHCO_3$/1.25 $NaH_2PO_4$/3 KCl, and 25 dextrose/1 $MgCl_2$/2 mM $CaCl_2$, pH 7.3. Patch pipettes were fabricated from borosilicate glass (TW150F-6; WPI) to a resistance of 1–3 MΩ for mitral cell somatic recordings, and 8–10 MΩ for dendritic recordings. For dendritic recordings, we identified the first major branch point leading into the glomerular tuft under fluorescent microscopy in Thy1-YFP mice. Pipettes were filled with (in mM): 125 potassium gluconate/10 Hepes/4 Mg-ATP/0.3 Na-GTP/0.1 EGTA/10 phosphocreatine/0.05% biocytin/1:1,500 Alexa Fluor 594 hydrazide, adjusted to pH 7.3 with KOH. For some experiments, synaptic currents were blocked with 100 $\mu$M DL-2-amino-5-phosphonopentanoic acid (D,L-AP-5), 10 $\mu$M 2,3-dioxo-6-nitro-1,2,3,4-tetrahydrobenzoquinoxaline-7-sulfonamide (NBQX), and 5 $\mu$M gabazine (Ballwin). In other experiments, we used the gap junction blocker carbenoxolone (CBX; 100 $\mu$M). Because CBX can inhibit AMPA-mediated excitatory postsynaptic currents (EPSCs) (2), CBX was always used in the presence of NBQX to avoid nonspecific effects of CBX. Cyclothiazide (CTZ; 100 $\mu$M) or DL-*threo*-$\beta$-benzyloxyaspartic acid (TBOA; 25–100 $\mu$M) were added to the extracellular solution in some experiments. Current signals recorded with a Multiclamp 700A amplifier (Molecular Devices) were filtered at 2 kHz using a built-in Bessel filter and digitized at 10 kHz. Data were acquired using Axograph. Data acquisition was terminated when series resistance was >15 MΩ. For voltage clamp recordings, mitral cells were held at −60 mV. Mitral cells in current clamp were held at −58 to −65 mV by continuous current injection. Input resistances were calculated from hyperpolarizations evoked by inward current pulses (500–1,000 ms) used to test the steady state coupling coefficients, as well as 125 pA current test pulses. We used the peak voltage deflection during the hyperpolarization to calculate input resistance.

**Immunohistochemistry and Morphological Measurements.** After whole-cell recording, slices were fixed in 4% paraformaldehyde/PBS (72 mM $NaH_2PO_4$/28 mM $Na_2HPO_4$, pH 7.2) overnight at 4 °C. Slices were then permeabilized with 0.4% Triton X-100/PBS for 30 min at room temperature followed by PBS wash (3 times; 10 min). Biocytin fills were incubated with streptavidin conjugated with Alexa Fluor 598 (1:1,000; Molecular Probes) overnight at 4 °C. After PBS washing (3 times; 10 min), slices were mounted on slides with ProLong Antifade (Invitrogen), and imaged on a confocal microscope (Olympus) with a 20× objective. For measurements of apical dendrites and glomerular diameter, fixed slices were imaged on a confocal microscope, and analyzed using the NeuronJ plug-in within ImageJ freeware.


1. Brunjes PC (1994) Unilateral naris closure and olfactory system development. *Brain Res Brain Res Rev* 19:146–160.
2. Tovar KR, Maher BJ, Westbrook GL (2009) Direct actions of carbenoxolone on synaptic transmission and neuronal membrane properties. *J Neurophysiol* 102:974–978.

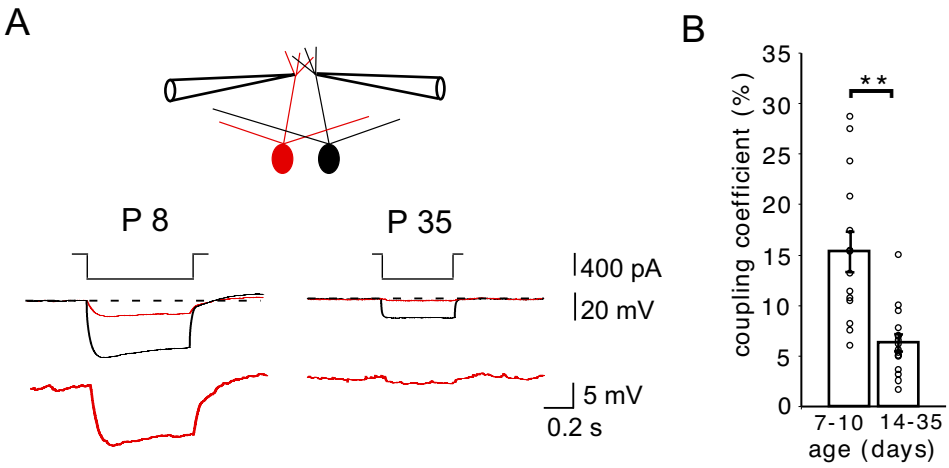


**Fig. S1.** Electrical coupling of mitral cell pairs using dendritic recordings. (*A*) Paired recordings in apical dendrites showed a similar decrease in coupling coefficients between P8 and P35 as in somatic recording. Hyperpolarizing current injection (−400 pA, 0.5–0.7 s) into the dendrite of cell 1 (black) elicited a voltage deflection in the dendrite of cell 2 (red). (*B*) The dendritic coupling coefficient at P7–10 was larger than at P14–35 (15.5 ± 2.0 vs. 6.0 ± 1.0; $P < 0.001$).

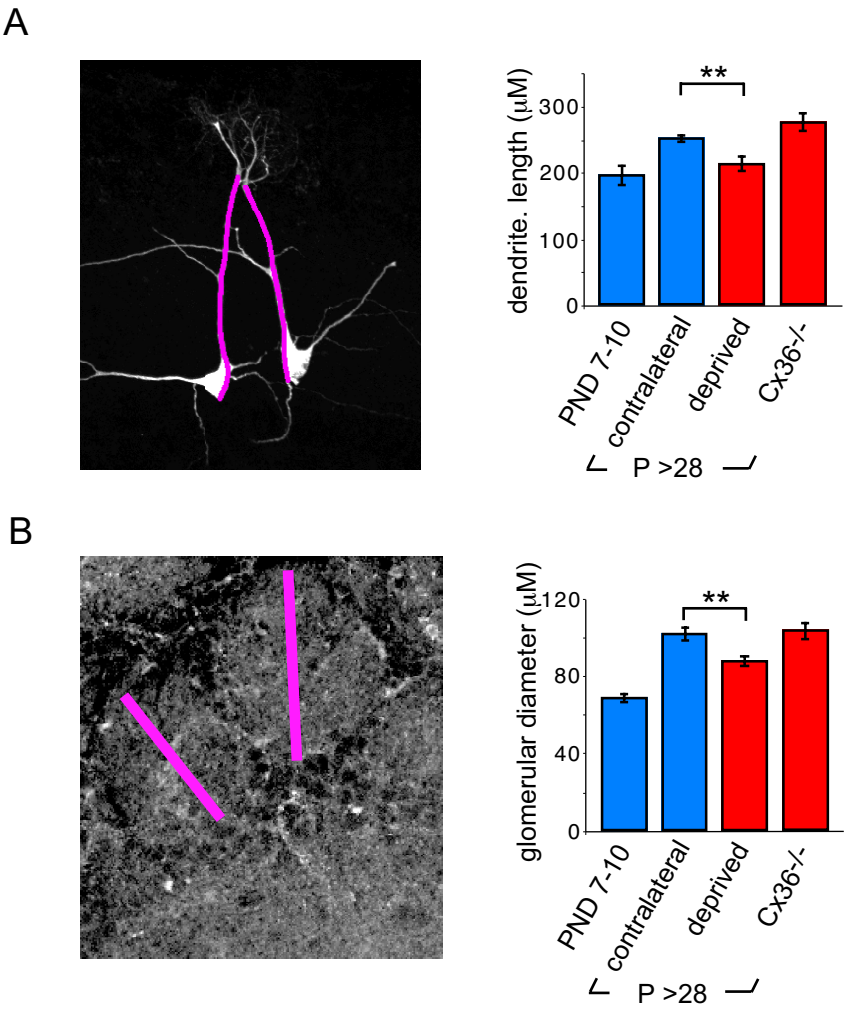


**Fig. S2.** The length of apical dendrites and glomerular diameters were smaller in sensory deprived bulbs compared with the contralateral side. (*A* and *B*) To assess the overall growth of mitral cells, we measured apical dendritic lengths and the diameter of glomeruli for young mice (P7–10) and for 3 groups at P > 28: sensory deprived, contralateral control, and connexin (Cx)36$^{-/-}$. Mitral cells were either filled with biocytin or imaged in Thy1-YFP mice as described in *Methods*. Slices were cut at 290 $\mu$m, fixed, and imaged on a confocal microscope. Cells with intact dendritic tufts were traced using Neuron J (Image J, National Institutes of Health) to calculate the length of apical dendrites as indicated by the red traces (*A Left*). Because the soma tapers into the apical dendrite, we included the soma diameter in the apical dendritic length measurement to avoid ambiguity. The sections were not cleared, and no corrections were made for fixation-induced shrinkage. Glomerular diameters were taken as the maximum diameter at the midpoint of a glomerulus in the Z-stack image (*B Left*). The histograms at right show the length of the apical dendrites and glomerular diameters from young animals (P7–10); and from young adult animals (P > 28) in control contralateral, sensory-deprived, and in Cx36$^{-/-}$ bulbs. Apical dendritic length and glomerular diameter were reduced in sensory-deprived compared with the contralateral control bulbs (dendritic length: 214.8 ± 10.9 vs. 254.6 ± 4.5 $\mu$m, $P < 0.005$; glomerular diameter: 88.9 ± 2.7 vs. 102.4 ± 3.2, $P \leq 0.001$. The Cx36$^{-/-}$ measurements did not differ from contralateral control ($P = 0.24$ and $P = 0.76$). Sample size in the 4 groups of animals ranged from 5 to 33.

A

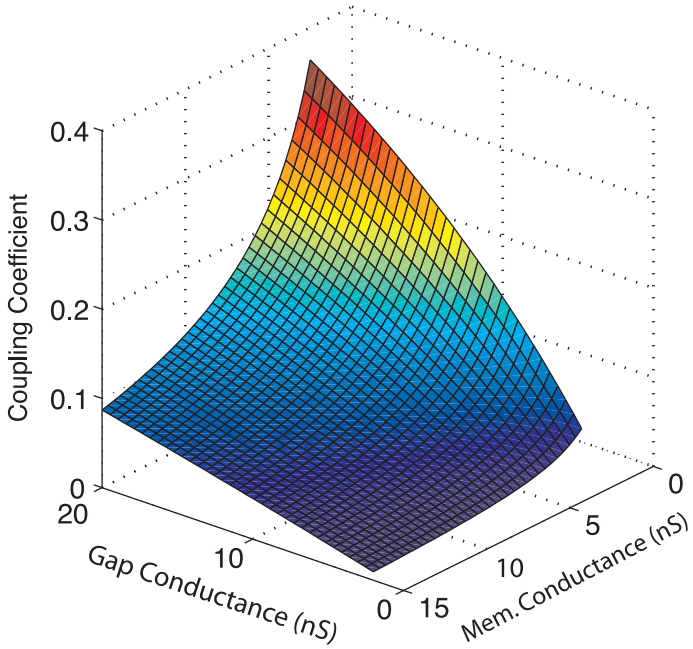


B

| | Gm (nS) | Gg (nS) | Coupling Coefficient |
|---|---|---|---|
| **P7-P10 Pairs** | 4.0 ± 0.2 | 8.3 ± 1.3 | 0.124 ± 0.013 |
| **P7-P10 Carb.** | 9.9 ± 1.1 | 3.7 ± 0.9 | † |
| **Deprived** | 8.4 ± 0.7 | 14 ± 2 | 0.105 ± 0.014 |
| **>P21 Pairs** | 25.0 ± 1.7 | 9.3 ± 1.1 | 0.037 ± 0.005 |
| **>P21 Carb.** | 16.7 ± 1.4 | 4.5 ± 1.2 | † |
| **Contralateral** | 31 ± 4 | 17 ± 4 | 0.041 ± 0.008 |

**Fig. S3.** Simulations of the relationship between the coupling coefficient, gap-junctional conductance, and the membrane conductance. We constructed a network model representing 15 mitral cells connected by gap junctions to examine what factors give rise to the measured differences in the coupling coefficient between ages, and as a result of sensory deprivation (see *SI Appendix*). We started with a model that had uniform connectivity, i.e., every cell connects to every cell with the same gap-junctional conductance. (*A*) General model predictions. The surface plot shows the predicted dependence of the coupling coefficient on the gap-junctional conductance and the non-gap-junctional membrane conductance (Eq. **s3.3** in *SI Appendix*). The coupling coefficient in the model is determined not only by the strength of gap junctions between a pair of mitral cells, but also by the membrane conductance (Eq. **s3** in *SI Appendix*). Specifically, the coupling coefficient decreased as gap-junctional conductance decreased for a given membrane conductance, but also decreased as membrane conductance increased for a given gap-junctional conductance. For 3 additional modeling schemes, we incorporated variability in the strength of gap junctions (uniform or biased random distributions). In these schemes, the average gap conductance (Eq. **s8.1**–**s8.3** in *SI Appendix*) and membrane conductance followed the same relationship to the average coupling coefficient as for the uniformly connected case (Eq. **s7** in *SI Appendix*). The coupling coefficient was correlated to the strength of the gap-junctional conductance between any 2 cells, but there was a substantial coupling coefficient even for cells with a very weak gap-junctional connection. The latter was the result of indirect gap-junctional interactions. (*B*) Experimental estimates. Using the uniform connectivity model (15 cells in the glomerulus, no randomness), we extracted an estimate of the gap-junctional conductance ($G_g$), and of the membrane conductance ($G_m$) for each pair of recorded neurons (Eq. **s2.1** and **s2.2** in *SI Appendix*). For the CBX experiments, we measured the membrane conductance in single cell experiments, and then, we estimated the gap-junctional conductance using the model to account for the effects of driving force (Eq. **s2.2** in *SI Appendix*). A comparison of the data in different experimental conditions revealed that a low coefficient was associated with a large membrane conductance, whereas the coupling coefficient and gap conductance did not correlate across conditions. $G_m$ in young animals (4 ± 0.2 nS, P7–10, $n = 24$) was smaller than in young adult animals (25 ± 2, P > 21, $n = 66$, $P < 0.0001$). Likewise $G_m$ in sensory-deprived animals (8.4 ± 0.7 nS, P > 28, $n = 22$) was smaller than in the contralateral controls (31 ± 4 nS, $n = 18$, $P < 0.0001$). In contrast, $G_g$ (at P7–10 and P > 28) calculated from CBX-treated cells was not significantly different (3.7 ± 0.9 nS vs. 4.5 ± 1.2, $P = 0.59$, $n = 6$ for both groups). Similarly, mitral cell pairs in control (8.3 ± 1.3 nS vs. 9.3 ± 1.1, $P = 0.6$, $n = 24$ and 66), as well as in naris-occluded and contralateral controls (14 ± 2 nS vs. 17 ± 4, $P = 0.5$, $n = 22$ and 18) showed no age- or experience-dependent effect on gap-junctional conductance. Coupling coefficients were not measured in CBX experiments (†, rightmost column).

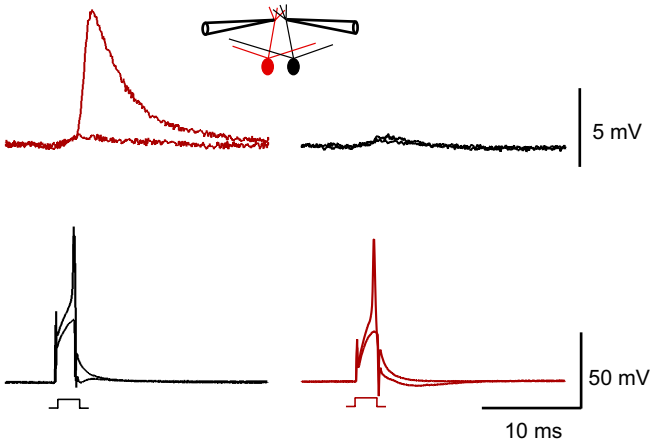


**Fig. S4.** Paired dendritic recording confirmed the presence of unidirectional mitral–mitral EPSPs. In recordings in the apical dendrite of mitral cells projecting to the same glomerulus ($P > 28$), short current injections (1.2 nA, 5 ms) in the dendrite of cell 1 (black, lower traces) produced a bAP that evoked a large mitral–mitral EPSP in the dendrite of cell 2 (red, middle traces). A subthreshold depolarization caused only a very small depolarization. However, when stimulating the cell pair in the opposite direction, a bAP in cell 2 (red, lower traces) evoked a depolarization that was no larger than produced by a subthreshold depolarization in cell 1 (black, upper traces), indicating the lack of direct spike coupling in these young adult animals and the unilateral expression of a mitral–mitral EPSP.

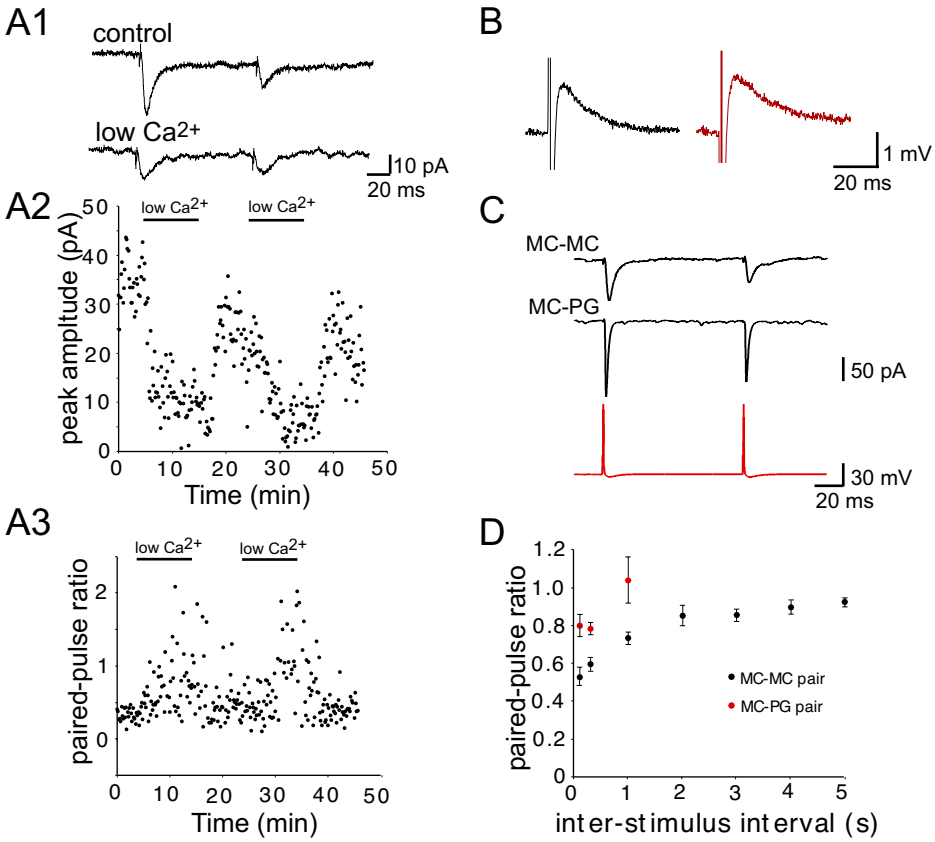


**Fig. S5.** Properties of mitral–mitral EPSCs. (*Ai–Aiii*) Mitral–mitral EPSCs were evoked by paired stimulation (interstimulus interval 100 ms). Reducing the extracellular calcium from 2.0 to 0.75 mM reversibly reduced the amplitude of the EPSC. Low calcium perfusion also increased the paired-pulse ratio. (*B*) An AMPA autoreceptor potential was present in both mitral cells regardless of whether they had a mitral–mitral EPSC, indicating that both dendrites could release glutamate. A subtraction protocol (before and after NBQX) was used to isolate the autoreceptor response. (*C*) The EPSC between 2 mitral cells showed greater paired-pulse depression than the EPSC between a mitral cell and a periglomerular interneuron. (*D*) The paired pulse ratio was plotted as a function of interstimulus interval for mitral–mitral EPSCs (black symbols) and for mitral-periglomerular EPSCs (red symbols).

## Other Supporting Information Files

*SI Appendix* (PDF)